Open access • Journal Article • DOI:10.1063/1.3439685

Atmospheric pressure plasma jet in Ar and Ar/H2O mixtures: Optical emission spectroscopy and temperature measurements — Source link

Abdollah Sarani, Anton Nikiforov, Christophe Leys

Published on: 17 Jun 2010 - Physics of Plasmas (American Institute of Physics)

Topics: Atmospheric-pressure plasma, Argon, Atmospheric pressure, Water vapor and Plasma diagnostics

Atmospheric pressure plasma jet in Ar and Ar/H_2O mixtures: Optical emission spectroscopy and temperature measurements

Abdollah Sarani,[1,a)] Anton Yu. Nikiforov,[1,2] and Christophe Leys[1]
[1]*Department of Applied Physics, Ghent University, Jozef Plateaustraat 22, Ghent B-9000, Belgium*
[2]*Institute of Solution Chemistry, RAS, Academicheskaya Str., 1, Ivanovo 153045, Russia*

(Received 9 February 2010; accepted 10 May 2010; published online 17 June 2010)

An atmospheric pressure plasma jet generated in Ar/water vapor mixtures has been investigated and the effect of water content on plasma properties has been studied. Plasma generated in Ar/water (0.05%) mixture shows higher intensity of OH radicals in emission spectra than pure argon alone. Plasma density has been estimated from current measurement and is in order of 1.5×10^{13} cm^{-3}. Electron temperature has been estimated as 0.97 eV in pure Ar and it decreases with an increase in water content in plasma. The gas temperature has been determined by fitting of the experimental spectra and using the Boltzmann plot method. The gas temperature increases with the addition of water to feed gas from 620 K in pure Ar up to 1130 K for 0.76% H_2O. © *2010 American Institute of Physics*. [doi:10.1063/1.3439685]

I. INTRODUCTION

Nonthermal and low temperature plasmas are a subject of great interest in different fields of science and applications. Atmospheric pressure plasma jets attract high attentions because of their potential interest for different technologies, such as polymer treatment, as well as of fundamental investigations of plasma.[1–3] Up until now few atmospheric pressure plasma systems have been developed such as rf or microwave torch[3–6] and arc discharges.[7] This paper presents a continuation of our work[8] that has been carried out on ac sustained plasma jet with focuses on studying the effect of addition of water to inlet gas. Potential applications of investigated plasma jet are to modify the surface properties of different polymers (even in three-dimensional and nonplanar), cleaning of substrates and biomedical applications.[9] Dielectric barrier discharges working with either sinusoidal signals around 10–100 kHz, where the dielectric prevents the formation of the high temperature arcs, are the most common atmospheric pressure system currently in use.[10] In this particular plasma source, the diameter of quartz capillary (and consequently, interelectrode gap) was reduced in order to obtain stable plasma with long afterglow zone. Commonly used technique for atmospheric pressure discharges investigations is optical emission spectroscopy (OES).[11] A number of groups estimate excitation temperature[12] from ratio of relative intensity of atomic lines in suggestion that this value is similar to electrons temperature in the discharge. Another application of the emission spectroscopy is to measure gas temperature by fitting of the rotational/vibrational spectra of hydroxyl radicals or nitrogen second positive system and simulated one with variation in translation temperature of the system.[13] Critical review of this technique was presented by Bruggeman[14] in case of plasma in contact with liquid electrode where concentration of water vapor in gas phase is relatively high in comparison with plasma jet systems. In the present paper the influence of water content on plasma parameters has been studied and validation of different techniques for gas temperature measurements have been discussed.

II. EXPERIMENTAL PROCEDURE

An atmospheric pressure plasma jet was generated in a quartz capillary with inside and outside diameters of 1.3 and 3.0 mm, respectively. Figure 1 shows the experimental setup used in this work.

The system consists of two electrodes, in which one electrode is insulated from another by dielectric material. The high voltage electrode is a rod of 0.5 mm diameter with half spherical shape of the tip. The electrode is made of tungsten and placed inside the quartz capillary. The ground electrode is in form of a ring with length of 10 mm which is placed around the capillary. The distance between the ground electrode and tip of high voltage electrode is 40 mm and the ground electrode is placed 20 mm away from the edge of the capillary. High purity Ar with main impurity H_2O at range of 0.3 ppm has been used for plasma generation at the flow range from 0.695 to 4.82 slm (slm denotes standard liters per minute). The gas flow was controlled by mass flow controllers model MKSPR400. The concentration of the water vapor content in the system is controlled by a bubbling system with distilled water. In this work the water content in mixture with Ar was set from 0.05% to 0.76% by changing of the gas flow passing the bubbler. By flowing gas through the tube between these two electrodes plasma jet is generated on sinusoidal wave voltage at fix frequency of 71 kHz. The applied voltage peak to peak value was varied between 12.2 and 17 $kV_{p.p.}$. The input power has been kept constant in all experiments as 12.8 W. The voltage waveform has been recorded by Tektronix TDS 1002 digital oscilloscope with a high voltage probe P6015A. The current was measured by a current transformer (Ion Physics model CM-100L) on the high voltage side. The sensitivity of the current probe at the frequency range from 600 Hz up to 200 MHz is 1 V/A. The fast imaging has been done with a Hamamatsu intensi-

a)Electronic mail: abdollah.sarani@ugent.be.

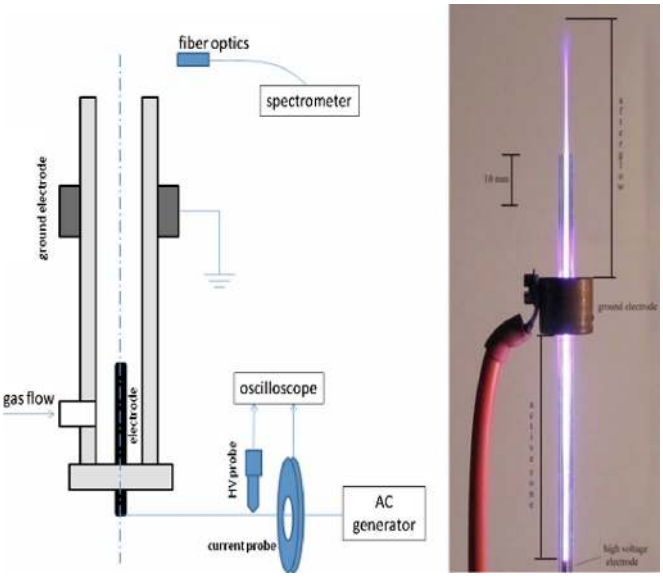

FIG. 1. (Color online) Experimental setup and visual view of the plasma jet.

fied charge-coupled device (ICCD) camera model C8484. Optical emission spectra of the discharge in the region of 250–900 nm has been recorded by Ocean Optics spectrometer with low resolution 0.7 nm and partially resolved spectrum of OH radicals emission 300–350 nm has been obtained with Avantes spectrometer at resolution 0.05 nm.

III. RESULTS AND DISCUSSION

A. Electrical characteristics and dynamic of plasma jet

In all mixtures, at an applied voltage of less than 8 kV (peak to peak value), only a weak radiation zone is observed inside the capillary, on the edge of the high voltage electrode. This discharge is similar to a well-known corona discharge. Furthermore, an increase in the applied voltage results to complete breakdown of interelectrode gap and formation of bright plasma between electrodes with afterglow up to 40 mm. The influence of water content on discharge electrical characteristics has been studied by the Lissajous voltage-charge plots. Example of V/C plots for fixed voltage 12.4 $kV_{p.p.}$ is shown in Fig. 2, where the area corresponds to energy input per cycle.

The Lissajous figures show that the discharge voltage and current waveforms are symmetrical for both polarities of the applied voltage. Addition of water vapor results to a decrease in the width of current peaks and an increase in current peak value. In case of pure Ar, two peaks on the plasma jet current waveform can be distinguished. The durations of the pulses are estimated as 0.4 and 2.8 μs for first and second pulses, respectively. Addition of water vapor at 0.05% concentration to the feed gas results to an increase in maximum current value of up to 50 mA and a decrease in pulses duration. It is interesting to note that current waveform at highest water vapor concentration is not symmetrical for different polarities of the applied voltage. The Lissajous figures clearly show that power dissipation during positive half period of the applied voltage is higher than negative cycle.

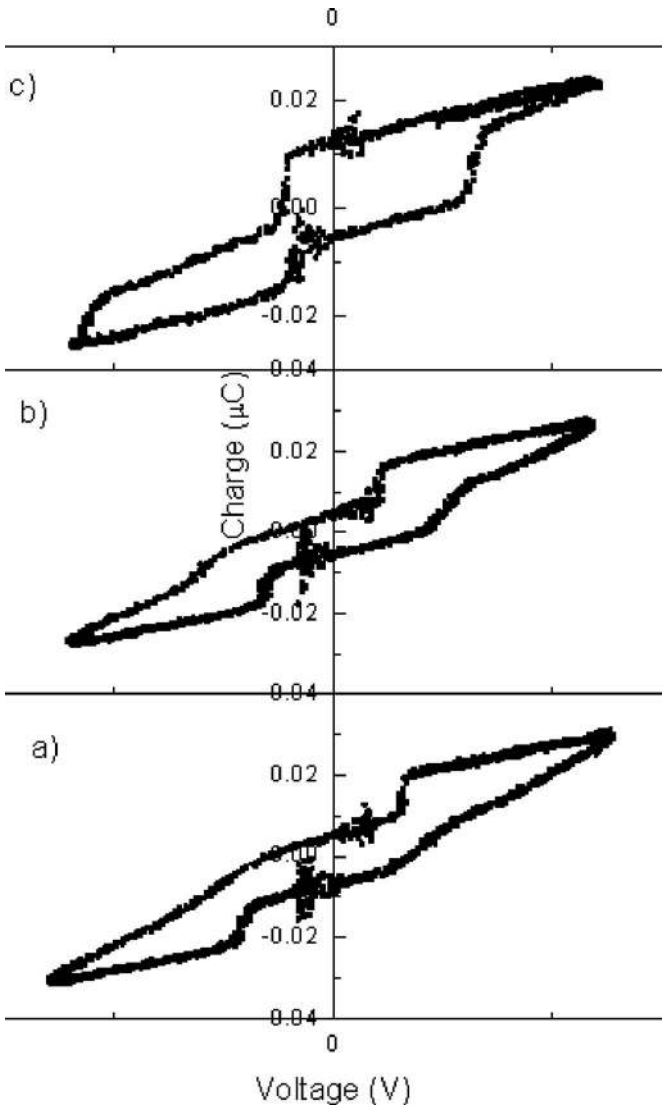

FIG. 2. Lissajous diagram showing the voltage-charge variation in DBD plasma jet (a) pure Ar, (b) Ar/H_2O 0.05%, and (c) Ar/H_2O 0.76%.

Plasma dynamics in the afterglow of the jet has been studied using ICCD technique with an exposition time of 20 ns. In Fig. 3, images of discharge are presented. Experiments have shown that the discharge in Ar or Ar/H_2O mixtures is generated in filamentary mode. Every current pulse on current waveform of the jet corresponds to formation of one filament. Also, it was found that in Ar/H_2O mixtures (at the range of 0.05%–0.76%), presence of water vapor in inlet gas does not influence life time and dynamics of the filament. Propagation time of filament can be estimated from ICCD images and in Ar/H_2O mixtures and it is about 150 ns. Diameter of the filament is close to diameter of the quartz capillary. The main distinguishing feature at highest water content is a small filament intensity on negative half period of applied voltage. This is due to asymmetry behavior of current waveform on positive and negative half periods of discharge at H_2O content of 0.76%.

An estimation of filament diameter allows us to determine maximal concentration of electrons from current density (peak value) at known mobility of electrons as

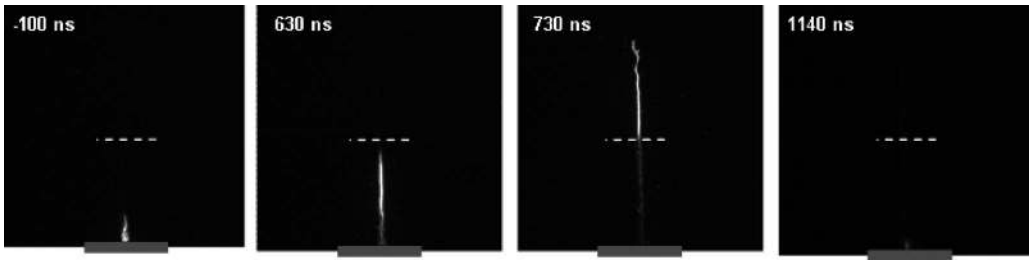

FIG. 3. ICCD images of plasma afterglow in Ar gas at 12.2 $kV_{p.p.}$. Time, presented in the left corners of the images, is related to moment where the current of the discharge reaches maximum value.

$$J = n_e e v_e \left(\frac{E}{N}\right) = n_e e \mu_e E, \tag{1}$$

where J is the current density, e is the elementary charge in I s^{-1}, E is the electrical field in V m^{-1}, and μ_e is the mobility of electron in argon gas. The experimental value of electron mobility in argon ($\mu_e p = 0.23 \times 10^6$ cm^2 Torr/V s $\Rightarrow \mu_e = 0.03$ m^2/V s) is obtained from Ref. 15. Using Eq. (1), the electron density in pure Ar jet in the filament is estimated as 1.5×10^{13} cm^{-3}.

An increase in water content in plasma results to a decrease in electron density due to a higher rate of electron collisions with molecular species. However, correct estimation of this effect requires knowledge of electron mobility in Ar/H_2O mixtures.

B. Optical emission spectroscopy

OES appears as a common technique used in determining discharge parameters,[16] especially, in the UV/visible region for determining neutral gas temperature. Axial OES of the jet with resolution of 0.7 nm has been applied for characterization of the afterglow. An overview of axial spectra is shown in Fig. 4.

Most intensive emission lines are listed in Table I. The discharge produces a significant UV radiation which belongs to transitions of the OH band at 308 and 287 nm $[A\ ^2\Sigma^+(v=0,1) \rightarrow X^2\Pi(v=0)]$. Apart from those lines the other most important features correspond to the atomic oxygen and N_2 species, which are located at 777.4 and 844 nm (O^I line) and 310–440 nm (N_2 bands).

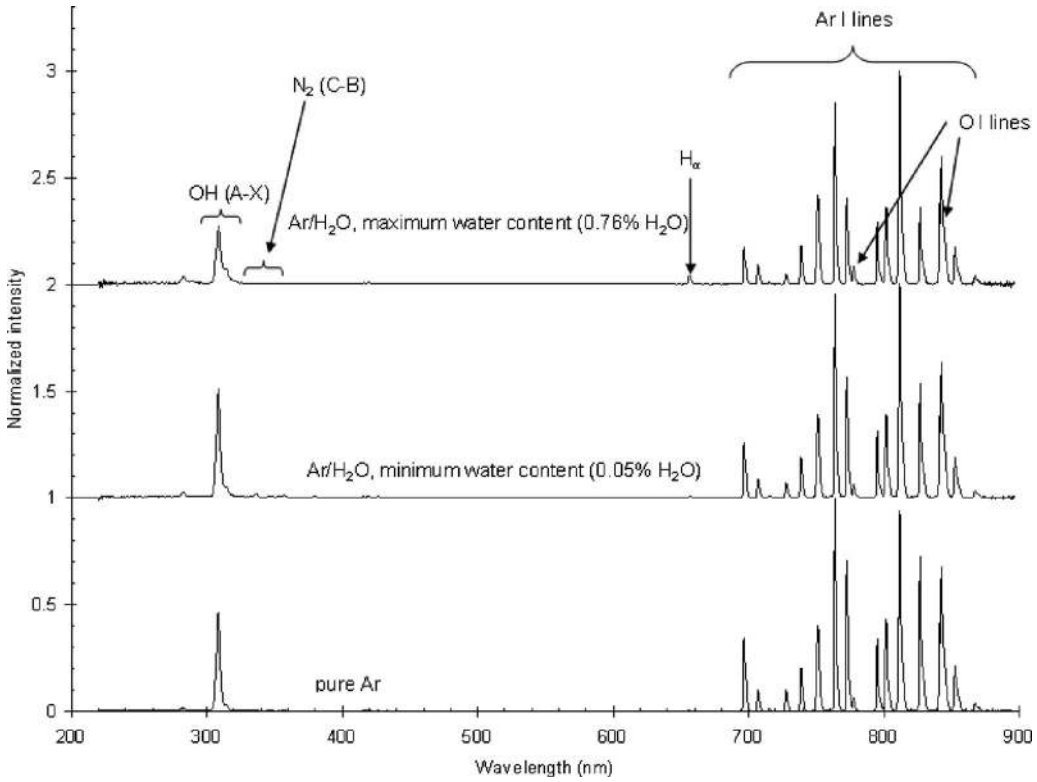

FIG. 4. Axial emission spectra of the jet in Ar and Ar/H_2O mixtures with 0.05% and 0.76% H_2O. The input power is fixed on 12.8 W. Spectra are shifted for better representations.

TABLE I. Most intensive emission lines which detected in axial spectra of the jet.

Species	λ (nm)	Transition	*E* (eV)	*J-J′*	*g-g′*
Ar I	696.54	$3s^23p^5(^2P^0_{3/2})4s$-$3s^23p^5(^2P^0_{1/2})4p$	13.32	2-1	5-3
Ar I	751.46	$3s^23p^5(^2P^0_{3/2})4s$-$3s^23p^5(^2P^0_{3/2})4p$	13.27	1-0	3-1
Ar I	763.51	$3s^23p^5(^2P^0_{3/2})4s$-$3s^23p^5(^2P^0_{3/2})4p$	13.17	2-2	5-5
Ar I	772.42	$3s^23p^5(^2P^0_{1/2})4s$-$3s^23p^5(^2P^0_{1/2})4p$	13.32	0-1	1-3
Ar I	801.47	$3s^23p^5(^2P^0_{3/2})4s$-$3s^23p^5(^2P^0_{3/2})4p$	13.09	2-2	5-5
Ar I	811.53	$3s^23p^5(^2P^0_{3/2})4s$-$3s^23p^5(^2P^0_{3/2})4p$	13.07	2-3	5-7
Ar I	826.45	$3s^23p^5(^2P^0_{1/2})4s$-$3s^23p^5(^2P^0_{1/2})4p$	13.32	1-1	3-3
Ar I	842.46	$3s^23p^5(^2P^0_{3/2})4s$-$3s^23p^5(^2P^0_{3/2})4p$	13.09	1-2	3-5
O I	777.41	$2s^22p^3(^4S^0)3s$-$2s^22p^3(^4S^0)3p$	10.74	2-2	5-5
O I	844.63	$2s^22p^3(^4S^0)3s$-$2s^22p^3(^4S^0)3p$	10.98	1-2	3-5
H_α	656.28	2p-3d	12.08	3/2-5/2	4-6
N_2	337.1	$(C\ ^3\Pi_u - B\ ^3\Pi_g)$			
OH	287	$A\ ^2\Sigma^+ \rightarrow X\ ^2\Pi,\ \Delta v=1$			
OH	308	$A\ ^2\Sigma^+ \rightarrow X\ ^2\Pi,\ \Delta v=0$			

An increase in water content results from a decrease in all atomic line emission in a whole spectral range (Figs. 4 and 5). This can be correlated with a decrease in electron temperature at higher water content. As can be seen from Fig. 5, the emission of Ar lines at 696, 763, and 801 nm decreases at almost the same rate but O^I (777 nm) emission decreases at a much faster rate. The required energy to produce O^I (^5P) from H_2O is 15.9 eV while the energy for Ar excitation is about 13.08–13.33 eV (depending on the transition). Hence, a decrease in T_e with growth of water content will affect the intensity of O^I stronger than Ar lines, which is in good agreement with our experimental results. This means that the main mechanism of decreasing atomic line intensity at higher water content is probably an increase in energy transfer between electrons and heavy species with addition of molecular species, such as H_2O that causes a reduction in T_e. A decrease in OH radical band emission in the discharge is not linear. Maximum emission is observed when the water content in the discharge was about 500 ppm. Furthermore, a decrease in OH band intensity at higher water content is due to high efficiency of radicals quenching with water vapor as it was suggested in Refs. 17 and 18 and also by a decrease in electron temperature in the system. Indirect evidence of high efficiency of OH radicals quenched by H_2O in Ar plasma can be observed from the Boltzmann distribution of OH radicals emission band (*A-X*). Afterward it will be shown a strong overpopulation of OH vibrational-rotational distribution at high rotational levels with $J>13$ is growing with an increase in water content in the plasma. The enhancement of the overpopulation of high excited levels of OH radicals with an increase in H_2O content is explained by the difference in quenching rates for different rotational levels. It was found in Ref. 19 that the quenching rate decreased by a factor of 1.5 with an increase in rotational excitation from $J=0$ to $J=10$. As a result, such process leads to growth of the overpopulation of rotational distribution with $J>13$, which is because of an increase in H_2O in feed gas.

In order to estimate gas temperature along the jet the optical emission profiles were recorded in whole afterglow with space resolution of 1 mm. Figure 6 shows spatially resolved optical emission intensities of Ar/H_2O with 0.76% of H_2O.

The result of space resolved OES shows that in both Ar/H_2O mixtures there is an important drop in the intensity of the Ar lines when the water is injected in feed gas. This is a well-known effect of the presence of molecular gases in noble gas plasma, and it has also been observed when other molecular species are inserted into the plasma.[16] An interesting feature that can be seen from space resolved OES Ar/H_2O mixtures is that in mixture with minimum amount of water, maximum emission of OH radicals is observed. One of the possible explanations of this effect has been suggested in our recent work.[8]

The presence of different Ar lines in spectrum of the afterglow allows us to estimate argon excitation temperature.

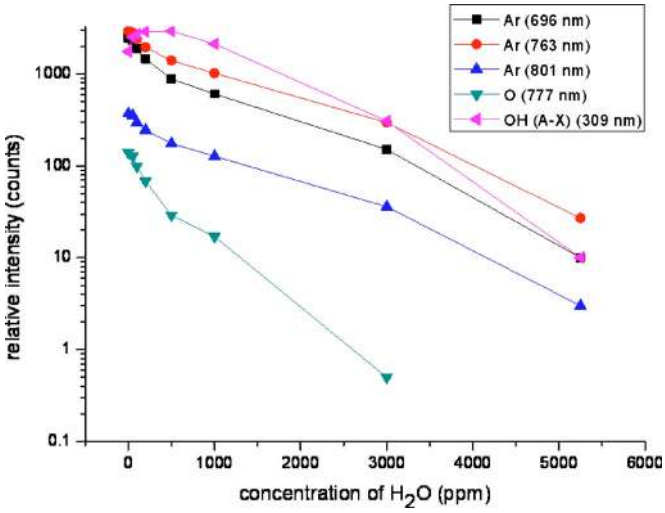

FIG. 5. (Color online) Peak emission intensity of excited species as a function of water content in the discharge (fixed power of 12.8 W).

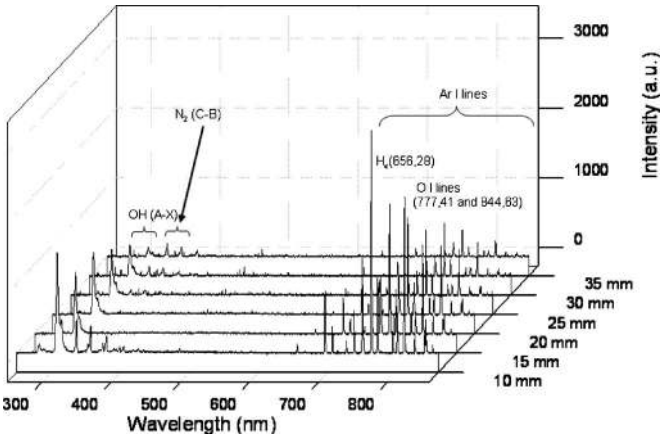

FIG. 6. Space resolved OES of Ar/H_2O plasma (0.76% H_2O) along with comparison of space resolved intensity of Ar, OH, and N_2 lines.

Up until now there is a wide discussion related to the comparison of excitation temperature T_{exc} with temperature of electrons T_e (Ref. 20–22) in different kind of discharges. It was shown that even in the case of local thermal equilibrium (LTE)[10,11] conditions T_e can be very different from estimated T_{exc}, which gives us only information about high energy tail of electron energy distribution function. T_{exc} can be evaluated from Eq. (2),[23]

$$N_j = \frac{g_j \exp(-E_j/k_B T_{exc})}{Z T_e}, \tag{2}$$

where k_B is the Boltzmann constant, N is the total population density, g_j is the statistical weight of upper level, and the denominator is the sum of the weighted Boltzmann functions of all the discrete energy levels. Without self-absorption of photons for atoms in the excited level j, which decay by radiative transfer to ground level i, the plasma emissivity ε_{ji}(W cm^{-3}) can be presented as

$$\varepsilon_{ji} = \frac{hc}{\lambda_{ji}} N_j A_{ji}, \tag{3}$$

where h is Planck's constant, c is the velocity of light in vacuum, A_{ji} is the probability of the transition $j \rightarrow i$, and λ_{ji} is the wavelength of the radiation.

It should be noted that at atmospheric pressure plasmas, self-absorption of argon lines alter the line ratios for different transitions in range of order of magnitude or even bigger.[24] It is possible that due to self-absorption, the error in estimated T_{exc} reaches a very high value because of exponential dependence of intensity ratio on T_{exc}. In the present study, in order to consider absorption of photons in Eq. (3), we used the method suggested by Schulze *et al.*[25] In the case of reabsorption plasma emissivity should be corrected by escape factor estimating the amount of the photons absorbed in plasma volume. Absorption of the photons for transition $i \rightarrow j$ along an optical path can be expressed by the escape factor

$$\gamma_{ij} = \Omega \theta_{ij} n_i, \tag{4}$$

where γ_{ij} is the escape factor, Ω is the solid angle, and θ_{ij} is the escape probability which states the value of the photons reduction due to self-absorption in plasma volume. The exact calculation of the escape factor (γ_{ij}) requires knowledge of spatial distribution of species density in lower states and experimental value of solid angle. The simplified model presented in Ref. 25 can be used in order to make estimations of escape factors in argon plasma. The latter is based on assumption of homogeneous profile for radiative species. Therefore, the escape factor can be expressed by the following equation:[26]

$$\gamma_{ij} \approx \frac{2 - \exp[-10^{-3} k_{ij}^0(\Delta\nu) l]}{1 + k_{ij}^0(\Delta\nu) l}, \tag{5}$$

where l is the length of plasma volume observed by the detector and $k_{ij}^0(\Delta\nu)$ is absorption coefficient in center of the line which has the following form:

$$k_{ij}^0(\Delta\nu) = \frac{\lambda_{ij}^2}{8\pi} P_{ij}(\Delta\nu = 0) \frac{g_i}{g_j} n_j A_{ij}, \tag{6}$$

where $P_{ij}(\Delta\nu)$ is a frequency distribution of the emission line determined by a broadening mechanism in experimental conditions. In atmospheric pressure plasma jet with $n_e < 10^{14}$ cm^{-3} and gas temperature of 620–1130 K, the Doppler broadening is negligible with respect to pressure broadening such as van der Waals. Such pressure broadening leads to a Lorentzian profile of atomic emission lines with full width half maximum (FWHM) δ_p. In our plasma conditions, $P_{ij}(\Delta\nu)$ can be determined by[27]

$$P_{ij}(\Delta\nu) = \frac{4}{\delta_p} \left[\frac{\delta_p}{4\pi(\Delta\nu - \beta_p)} \right]^2, \tag{7}$$

where β_p is a shift in central frequency in centimeters and δ_p is FWHM in centimeters which can be evaluated from the Lindholm–Foley theory,[28]

$$\delta_p(\text{cm}) = 16.36 \times 10^{-12} \lambda^2 (\bar{\alpha}\bar{R}^2)^{2/5} \left(\frac{T}{\mu} \right)^{3/10} N, \tag{8}$$

$$\beta_p = \tfrac{1}{3} \delta_p, \tag{9}$$

where μ is the reduced mass of the emitter-perturber system, N is the number density of the perturbed particles in cm^{-3}, and $\bar{\alpha}$ is the average polarizability of perturber in cm^{-3} which can be taken together with $\bar{R}^2$ from Ref. 29. The intensity of irradiation (measured in experiment value) corresponding to the plasma emissivity taking in to account absorption is defined by[30]

$$I_{ji}/\gamma_{ji} = \frac{\Omega V}{4\pi} \varepsilon_{ji} F_c, \tag{10}$$

where F_c is the correction function for sensitivity of the detector and V is the total plasma volume. Finally for the ratio of two emission lines (wavelengths λ_{ji} and λ_{kl}) by coupling Eqs. (2), (3), and (10) we obtain

$$\frac{I_{ji}}{I_{kl}} = \frac{\lambda_{kl} A_{ji} \gamma_{ij} g_j}{\lambda_{ji} A_{kl} \gamma_{lk} g_k} \exp\left(-\frac{E_j - E_k}{k_B T_e} \right). \tag{11}$$

Equation (11) allows estimating the T_{exc} of the emission source from intensity ratio of the same atoms of neighboring

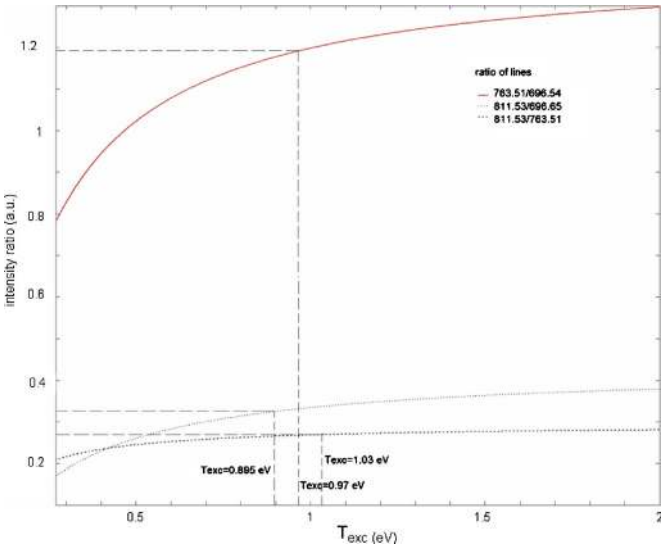

FIG. 7. (Color online) Logarithm of intensity ratio for different Ar lines as a function of T_{exc} considering correction for photon absorption.

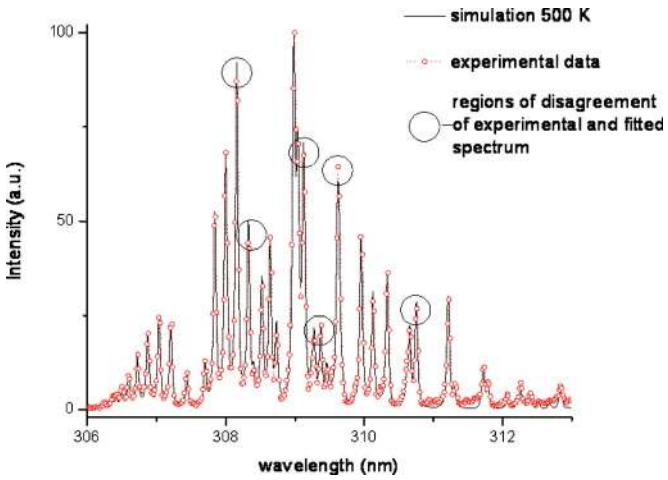

FIG. 8. (Color online) Fitting of the experimental and simulated spectrum of OH radical. $T_{rot}=450\pm25$ K, $T_{vib}=1800\pm250$, emission has been recorded in the position 5 mm after the edge of the capillary, pure Ar, and P=12.8 W.

ionization stages having similar excited state energies. In Fig. 7 line ratios corrected on reabsorption for three transitions, 696.54 nm $2p_2\rightarrow1s_5$, 763.51 nm $2p_6\rightarrow1s_5$, and 811.53 nm $2p_9\rightarrow1s_5$ (Paschen notation of the terms) are shown, which represent the example of the logarithm of the $I_{763.51}/I_{826.45}$ ratio as a function of T_{exc} for argon discharge.

The crossover points between the curve $\ln(I_{ji}/I_{kl})$ and the lines representing the measured ratio yield the desired excitation temperature of the plasma. The values of experimental lines ratio are 1.13, 0.33, and 0.27 for transitions $2p_6\rightarrow1s_5/2p_2\rightarrow1s_5$, $2p_9\rightarrow1s_5/2p_2\rightarrow1s_5$, and $2p_9\rightarrow1s_5/2p_6\rightarrow1s_5$, respectively, yielding to an excitation temperature of Ar 0.965 eV. The excitation temperature evaluated by line ratio technique taking into account the correction of the lines intensities due to self-absorption gives T_{exc}, which is in good agreement with estimations of other authors for argon discharges in atmospheric pressure, e.g., Refs. 3 and 31. Independent estimation of T_e and n_e in the argon discharge allows us to determine the deviation of the plasma from thermodynamic equilibrium by solution of the Saha equation,[27]

$$\frac{n_e n_z}{n_{z-1}} = 6.06\times10^{21}\frac{g_z}{g_{z-1}}T_e^{3/2}\exp(-\chi_{z-1}/kT_e), \qquad (12)$$

where χ_{z-1} is the energy required for ionization of state z in eV. It can be easily shown that using estimated temperature ($T_e=0.965$ eV) from the line ratio method in Eq. (12) results in very high electron density ($n_e>10^{19}$ cm^{-3}), which is impossible to reach in conditions of atmospheric pressure plasma jet. On the other hand, the solution of the Saha equation with $n_e=10^{13}$ cm^{-3} gives $T_e\leq0.5$ eV, which is two times lower than all experimental estimations of T_e.[3,31] Correspondingly, it can be shown that the argon plasma jet is far from LTE conditions and electrons are not reaching the quasiequilibrium state. The addition of water vapor to feed gas leads to an unexpected sharp decrease in T_e (e.g., only 0.2 eV in the case of 0.76% water content). This decrease is probably due to effective collisions of H_2O with excited argon species, which results in the drop of different argon line intensities where Eq. (11) is not more valid.

C. Gas temperature measurement

Because gas temperature is one of the key parameters in technological applications, great attention has to be given in its determination. The commonly used technique to estimate gas temperature is based on finding the best fit between experimental and simulated emission spectra of OH radicals or the second positive system of N_2. In this work firstly we determined T_{rot}^{OH} with the SPECAIR (Ref. 32) software. In Fig. 8 experimental and simulated spectra of OH radical emission (region 306–314 nm, resolution 0.05 nm) are presented. Fitting of the spectra is carried out with one rotational temperature and takes into account an instrumental function of the spectrometer. The rotational temperatures for pure Ar are 450 and 800 K in Ar/H_2O with maximum water content. It was found that, the rotational temperature is almost constant, in the afterglow of plasma jet. Unfortunately, the agreement between the experimental and simulated spectrum is improper at various wavelengths (shown on Fig. 8 by circles). Generally, it is impossible to determine precisely T_{rot} of OH radicals on the basis of the fitting procedure. An error in estimation of OH radical temperature increases with the growth of water content in the discharge as well.

Due to the importance of gas temperature, the second technique has been used for the correct estimation of the gas temperature. The Boltzmann plot of the rotational population of OH radicals as a function of the energy of levels is widely used for this purpose.[33,34] In Fig. 9, we presented $\ln[I\lambda/(2J+1)A_{JJ}]$ for transition OH($A\ ^2\Sigma-X\ ^2\Pi$) as a function of levels energy. This plot describes the distribution of OH($A\ ^2\Sigma$) radicals among rotational levels for Ar/water vapor mixture at discharge generated at fixed power of 12.8 W.

It is clear that transition OH($A\ ^2\Sigma-X\ ^2\Pi0,0$) shows a non-Boltzmann behavior. Similar distributions of OH radicals transition OH($A\ ^2\Sigma-X\ ^2\Pi$) are of a sufficiently general

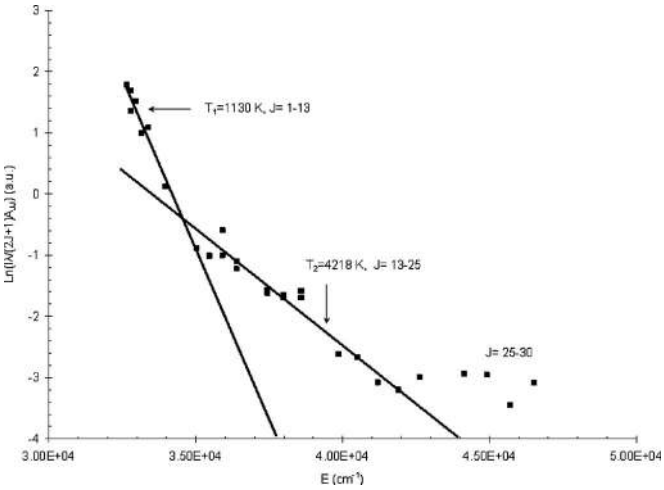

FIG. 9. Boltzmann plot of the OH (A-X) (0-0) transition in plasma of Ar/H_2O mixture containing 0.05% of water.

character and were widely observed in low pressure discharges and flames[35,36] and recently in a glow discharge with liquid electrodes generated at atmospheric pressure.[14] One can separate curves in three regions, e.g., for the low water content (0.05%) region of low temperature population with $J<13$ and $T_1=625$ K, region with $13<J<25$ characterized by much higher temperature $T_2=5000$ K, and region with $J>25$ characterized by fast depopulation of rotational-vibrational levels. Reasonable explanation of vibrational-rotational population of OH radicals can be due to different mechanisms of generation of excited species with different J numbers. We can suggest that excited OH radicals characterized by low rotational temperature are produced by electron impact excitation of ground state OH,

$$\mathrm{OH}(X\ ^2\Pi)+e\rightarrow \mathrm{OH}(A\ ^2\Sigma)^*+e \quad (E_{\mathrm{threshold}}=4\ \mathrm{eV}), \tag{13}$$

and at the same time there is a second independent mechanism of OH radical production by direct dissociation of water vapor,

$$\mathrm{H_2O}(X\ ^1A_1)+e\rightarrow \mathrm{H_2O}(B\ ^1A_1)+e \overset{\mathrm{dissoc}}{\rightarrow} \mathrm{OH}(A\ ^2\Sigma)^{**}+\mathrm{H}+e \quad (E_{\mathrm{threshold}}=10\ \mathrm{eV}), \tag{14}$$

where $\mathrm{OH}(A\ ^2\Sigma)^{**}$ radicals are at high excited levels. Hence, hydroxyl radicals characterized by high rotational temperature are generated almost exclusively by reaction (14) and radicals with lower rotational temperature are produced simultaneously by reactions (13) and (14). Both processes are independent and one can describe OH radicals distribution by two different temperatures, where the first one (at $J<13$) is equivalent to the gas temperature.[37] Population of radicals at levels with $J>25$ decreases fast due to the fact that the excitation energy of these levels is close to the predissociation of OH radicals.

As it is possible to see the determination of rotational temperature of OH radicals, it encounters technical difficulties in the interpretation of spectral data. Very well studied N_2 second positive system ($C\ ^3\Pi-B\ ^3\Pi$) is widely used for the same purpose especially in a case of atmospheric pressure discharges where N_2 is a main gas component.[30] Spectra of DBD jet generated in Ar and Ar water vapor mixtures show typical intensive bands of N_2 and N_2^+ in the afterglow of the jet even inside of capillary due to backdiffusion of surrounding air. Unfortunately, the presence of argon metastable atoms, e.g., Ar ($3p^54s$), in the afterglow results to nonresonance excitation of $N_2(C\ ^3\Pi)$ by the following mechanism:[37]

$$N_2(X\ ^1\Sigma)+\mathrm{Ar}^*\rightarrow N_2(C\ ^3\Pi)+\mathrm{Ar}, \tag{15}$$

along with overpopulation of rotational-vibrational levels of the nitrogen second positive system. Considering the above mechanism, determined rotational temperature of N_2 radicals has to be highly overestimated because of the absence of rotational equilibrium between N_2 radicals and other heavy species. It was found that $T_{\mathrm{rot}}^{\mathrm{N_2}}$ is about 1000 and 1500 K in the case of pure Ar jet and Ar/H_2O mixtures (0.76% H_2O), respectively (distance is 25 mm from ground electrode). This is much higher than the expected temperature and also the temperature of the jet which was determined from the Boltzmann distribution of OH radicals. On the basis of presented data concerning excitation mechanisms taking place in the afterglow zone, the rotational temperature of the system has been set equivalent to the temperature determined by the first slope of the Boltzmann plot of OH radicals in all investigated cases. Using the Boltzmann plot method, the OH rotational temperature has been determined. The results are presented in Table II. The rotational temperature in case of pure argon is around 625 K and 1100 K for maximum concentration of water in our experiments.

As can be seen in Table II, the temperature of the jet increases with the addition of water content in feed gas from 625 up to 1125 K. On the other hand it is important to note that gas temperature determined by fitting procedure is un-

TABLE II. The space resolved OH rotational temperature for Ar and Ar/H_2O mixtures determined by the Boltzmann plot technique. Error of the method is ±50 K.

	Active zone	Distance from ground electrode (mm)						
		5	10	15	20	25	30	35
$T_{\mathrm{rot}}^{\mathrm{OH}}$ (K), pure Ar	625	620	650	655	685	690	735	770
$T_{\mathrm{rot}}^{\mathrm{OH}}$ (K), Ar/H_2O 0.05%	620	625	610	625	640	725	740	1065
$T_{\mathrm{rot}}^{\mathrm{OH}}$ (K), Ar/H_2O 0.76%	1125	1135	1130	1130	1130	1130	1100	1020

derestimated in comparison with OH radical temperature, which was measured using the Boltzmann plot method. The explanation is two temperature distribution in the afterglow which does not take into account the fitting method. The smaller the rotational temperature the higher underestimation by fitting procedure is observed.

IV. CONCLUSION

Atmospheric pressure plasma jet generated in Ar/water mixtures is investigated and the effects of addition water on plasma properties have been studied. Axial and spatially resolved OESs have been done. Plasma discharge is filamentary with a lifetime of filament of 150 ns. Electron density has been estimated from current density and is of the order of 1.5×10^{13} cm^{-3}. Argon excitation temperature for pure Ar discharge is estimated to be 0.965 eV. The gas temperature is obtained from rotational temperature of the OH($A-X$) transition by two different methods: OH emission spectra fitting and the Boltzmann plot method. Using the first method is a matter of some difficulty due to bad fitting of the spectra. The reason is that three regions with different slopes (temperatures) of radicals exist on the Boltzmann distribution due to different mechanisms of OH radical production. The Boltzmann plot technique shows that gas temperature increases with the addition of water to inlet argon from 625 up to 1125 K (contains 0.76% water). Finally, it has been found that the maximum intensity of OH radicals in the discharge is observed in the mixture of Ar/water vapor (0.05% H_2O).

ACKNOWLEDGMENTS

This work was financially supported by the Belgian Program on Interuniversity Attraction Pole IAP-VI/08 (Project in Plasma Surface Interaction "PSI"-P6/08).

[1] S. Forster, C. Mohr, and W. Viol, Surf. Coat. Technol. **200**, 827 (2005).
[2] M. Laroussi, W. Hynes, T. Akan, X. Lu, and C. Tendero, IEEE Trans. Plasma Sci. **36**, 1298 (2008).
[3] J. L. Walsh, J. J. Shi, and M. G. Kong, Appl. Phys. Lett. **88**, 171501 (2006).
[4] M. Laroussi and T. Akan, Plasma Processes Polym. **4**, 777 (2007).
[5] X. Li, L. Dong, N. Zhao, Z. Yin, T. Fang, and L. Wang, Appl. Phys. Lett. **91**, 161507 (2007).
[6] A. Broc, S. De Benedictis, and G. Dilecce, Plasma Sources Sci. Technol. **13**, 504 (2004).
[7] X. Tu, B. G. Chéron, J. H. Yan, L. Yu, and K. F. Ce, Phys. Plasmas **15**, 053504 (2008).
[8] A.Yu. Nikiforov, A. Sarani, and C. Leys, "The influence of water vapor content on electrical and spectral properties of an atmospheric pressure plasma jet," Plasma Sources Sci. Technol. (unpublished).
[9] P. Rajasekaran, P. Mertmann, N. Bibinov, D. Wandke, W. Viöl, and P. Awakowicz, J. Phys. D: Appl. Phys. **42**, 225201 (2009).
[10] N. Balcon, A. Aanesland, and R. Boswell, Plasma Sources Sci. Technol. **16**, 217 (2007).
[11] H. R. Griem, *Principal of Plasma Spectroscopy (Cambridge Monograph on Plasma Physics)* (Cambridge University Press, Cambridge, 1997).
[12] J. L. Walsh and M. G. Kong, Appl. Phys. Lett. **93**, 111501 (2008).
[13] G. Herzberg, *Molecular Spectra and Molecular Structure I* (Van Nostrand, New York, 1950), p. 657.
[14] P. Bruggeman, D. Scharm, M. Á. González, R. Rego, M. G. Kong, and C. Leys, Plasma Sources Sci. Technol. **18**, 025017 (2009).
[15] K. K. Trusov, J. Phys. D: Appl. Phys. **40**, 786 (2007).
[16] A. Yanguas-Gil, K. Focke, J. Benedikt, and A. von Keudell, J. Appl. Phys. **101**, 103307 (2007).
[17] P. Bruggeman, F. Iza, P. Guns, D. Lauwers, M. G. Kong, Y. A. Gonzalvo, C. Leys, and D. C. Schram, Plasma Sources Sci. Technol. **19**, 015016 (2010).
[18] C. Hibert, I. Gaurand, O. Motret, and J. M. Pouvesle, J. Appl. Phys. **85**, 7070 (1999).
[19] C. B. Cleveland and J. R. Wiesenfeld, Chem. Phys. Lett. **144**, 479 (1988).
[20] Y. Yanguas-Gil, J. Cotrino, and A. R. Gonzalez-Elipe, J. Appl. Phys. **99**, 033104 (2006).
[21] X.-M. Zhu and Y.-K. Pu, Plasma Sources Sci. Technol. **17**, 024002 (2008).
[22] A. A. Garamoon, A. Samir, F. F. Elakshar, A. Nosair, and E. F. Kopt, IEEE Trans. Plasma Sci. **35**, 1 (2007).
[23] A. Chingsungnoen, J. I. B. Wilson, V. Amornkitbamrung, C. Thomas, and T. Burinprakhon, Plasma Sources Sci. Technol. **16**, 434 (2007).
[24] S. O. Kastner and A. K. Bhatia, J. Quant. Spectrosc. Radiat. Transf. **58**, 217 (1997).
[25] M. Schulze, A. Yanguas-Gil, A. von Keudell, and P. Awakowicz, J. Phys. D: Appl. Phys. **41**, 065206 (2008).
[26] R. Mewe, Z. Naturforsch. A **25A**, 1798 (1970).
[27] T. Holstein, Phys. Rev. **83**, 1159 (1951).
[28] E. Lindholm, Ark. Mat., Astron. Fys. **32**, 1 (1945).
[29] C. W. Allen, *Astrophysical Quantities*, 3rd ed. (Athlone, New York, 1973), p. 92.
[30] H. Nassar, S. Pellerin, K. Musiol, O. Martinie, N. Pellerin, and J. M. Cormier, J. Phys. D **37**, 1904 (2004).
[31] X. M. Zhu, W. C. Chen, and Y. Kang Pu, J. Phys. D: Appl. Phys. **41**, 105212 (2008).
[32] C. O. Laux, in *Physico-Chemical Modeling of High Enthalpy and Plasma Flows*, von Karman Institute Lecture Series No. 2002-07, edited by D. Fletcher, J.-M. Charbonnier, G. S. R. Sarma, and T. Magin (Rhode-Saint-Genèse, Belgium, 2002).
[33] K. P. Huber and G. Herzberg, *Molecular Spectra and Molecular Structure I* (Van Nostrand Reinhold, New York, 1979), Chap. V.
[34] B. A. Cruden and M. Meyyappan, J. Appl. Phys. **97**, 084311 (2005).
[35] J. P. Pichamuthu, J. C. Hassler, and P. D. Coleman, J. Appl. Phys. **43**, 4562 (1972).
[36] T. Carrington, J. Chem. Phys. **41**, 2012 (1964).
[37] V. N. Ochkin, S. Yu. Savinov, and N. N. Sobolev, in *Electronically Excited Molecules in Nonequilibrium Plasma*, edited by N. N. Sobolev (Nauka, Moscow, 1985), pp. 6–85 (in Russian).